Sensors and Materials, Vol. 23, No. 7 (2011) 381–396
MYU Tokyo

S & M 0854

Integration of p-n Junction Diode to Cantilever Mass Sensor for Frequency Drift Compensation due to Temperature Fluctuation

Tsuyoshi Ikehara*, Mitsuo Konno, Sunao Murakami,
Tadashi Fukawa[1], Mutsumi Kimura[1] and Takashi Mihara[2]

National Institute of Advanced Industrial Science and Technology (AIST),
1-2 Namiki, Tsukuba, Ibaraki 305-8564, Japan
[1]Faculty of Textile Science and Technology, Shinshu University,
3-15-1 Tokida, Ueda, Nagano 386-8567, Japan
[2]Future Creation Laboratory, Olympus Corporation,
2-3 Kuboyama-cho, Hachioji, Tokyo 192-8512, Japan

(Received January 17, 2011; accepted March 8, 2011)

Key words: chemical sensor, cantilever mass sensor, resonant frequency, silicon, micro-electromechanical systems (MEMS), temperature sensor, frequency drift

Silicon resonant sensors generally show frequency drift due to temperature fluctuation. A p-n junction diode was integrated to a resonant mass sensor using a silicon cantilever in one chip for frequency drift compensation due to temperature fluctuation. The diode could be fabricated by almost the same fabrication process simultaneously with piezoresistive stress gauges and showed good p-n junction characteristics for a temperature sensor. The sensor chip consisted of multiple cantilevers and the diode was assembled to a sensor package with a PZT vibrator and oscillated using a feedback electric circuit. Frequency drift trends under induced temperature changes could be almost compensated using the temperature read by the on-chip diode and a temperature coefficient. The temperature coefficients were −34 and −78 ppm/°C for gold-coated and polybutadiene-coated cantilevers, respectively, and found to depend strongly on the surface adsorption films on the sensor. Frequency drift compensation under a chemical sensing situation was also demonstrated, which was reduced from the original drift up to 30 Hz to almost 2 Hz. Temperature compensation using an on-chip temperature sensor is considered to be important for chemical sensing using silicon cantilevers where gas flows can easily change the temperature of the sensor.

*Corresponding author: e-mail: ikehara.t@aist.go.jp

1. Introduction

Sensors using the mass detection principle have been applied to chemical sensing because the use of various adsorption materials enables selective sensing. The quartz crystal microbalance (QCM) has been particularly utilized as the platform of mass sensing because of its high stability and adaptability to wide applications.[1] The QCM, a quartz thin disk sandwiched between metal electrodes, exhibits resonance of in-plane thickness-shear mode vibration typically at approximately 9 MHz. The resonant frequency of a QCM shifts when molecules are captured in the adsorption film coated on the quartz plate due to mass effect. Many types of adsorption material including polymers[2] and biomaterials[3] have been employed.

Recently, silicon resonators such as microcantilevers[4–8] and microdisks[9–11] have been proposed as a smart alternative to QCM because microfabrication technology is expected to realize much smaller and integrated mass sensors. Moreover, small size and thickness provide higher mass sensitivity owing to the smaller resonator mass.[12] Analysis functions are expected when multiple sensors with different adsorption materials are integrated in one chip, such as in human olfactory organs.

However, silicon has a drawback in that the temperature effects are larger than those of quartz. The resonant frequency of the silicon resonator changes at more than 10 ppm/°C owing to the change in its elastic properties,[13] whereas the rate can be suppressed to approximately 1 ppm/°C in quartz crystal by using an AT-cut vibration plate. Additionally, temperature effects due to surface layers such as metal wiring or oxide passivation films become significant when the structures are more miniaturized. Therefore, the compensation of temperature effects is generally inevitable for vibration-type sensors made of silicon, such as resonant accelerometers and resonant strain sensors. Either on-chip[14,15] or out-of-chip[16] temperature sensors are usually assembled for such sensors to compensate for temperature effects. As an on-chip temperature sensor, a p-n junction diode and a thin-film thermocouple have often been utilized.[17,18]

Despite the importance for silicon resonator devices, compensation techniques have not been reported often. Harada *et al.* have reported that an external temperature sensor was employed to integrate commercial pressure sensors using a silicon resonant strain sensor.[16] Lange *et al.* have already realized a cantilever mass sensor integrated with a complementary metal oxide semiconductor (CMOS) driving circuit in which a temperature sensor could be easily combined.[6] However, they did not describe temperature effects maybe because they had employed a thermal vibration excitation method. They reported that the increase in temperature was from 3 to 19°C from ambient temperature.

Temperature compensation is still a hot subject for MEMS applications. For the use of MEMS oscillators, active temperature control techniques using a micro-oven have been proposed.[19] These techniques are not suitable for cantilever chemical sensors because high-temperature operation can affect the ability of adsorption materials. The temperature compensation of silicon structures using surface oxide film has been reported.[20,21] Other methods have been reported, such as the modulation method using electrical feedback control,[22] comparison method of different resonance modes,[23]

and silicon property modification by doping.[24] These techniques can be applicable to mass sensors. We conjecture that almost all commercial silicon sensors possess a sort of temperature compensation function. However, no papers were found, as far as we know, dealing with the integration of the temperature sensor to a resonant mass sensor employing a silicon cantilever. As a result, the stability of chemical sensing against temperature change has not been well characterized.

In this study, a p-n junction temperature sensor was integrated on the same chip as a cantilever mass sensor and compensation of the frequency drift was investigated. The temperature effects on this sensor were expected to be different from those of encapsulated resonator devices because it had a surface polymer layer and was operated under a flowing air environment. This sensor chip was employed for an actual volatile organic compounds (VOCs) sensing experiment, and the advantages of the temperature compensation were examined followed by the basic characterization of the cantilever sensor.

2. Theory

2.1 *Temperature effects in silicon*

The temperature dependence of the resonant frequency of a silicon resonator is mainly dominated by elasticity in silicon. The resonant frequency f_i of the i-th flexural mode in a uniform isotropic cantilever with length l and thickness t is expressed as

$$f_i = \frac{\lambda_i^2 t}{2\pi l^2}\sqrt{\frac{E}{\rho}}, \tag{1}$$

where E and ρ are the Young's modulus and mass density of the cantilever material, respectively. The coefficients λ_i depend on the vibration mode order; $\lambda_1 \approx 1.875$, $\lambda_2 \approx 4.694$, $\lambda_3 \approx 7.855$, $\lambda_4 \approx 11.00$, ...[25] Young's modulus E has the largest temperature dependence among these parameters.

In single-crystal silicon (SCS), Young's modulus has orthotropic anisotropy owing to its cubic crystal nature. However, we can use eq. (1) because only the Young's modulus in the longitudinal direction is effective in the case of small deformation approximation. Young's modulus in specific direction cosine (l, m, n) under a crystal-axis coordinate system is expressed as[26,27]

$$E^{-1} = s_{11} - 2\left(s_{11} - s_{12} - \frac{s_{44}}{2}\right)(l^2m^2 + m^2n^2 + n^2l^2), \tag{2}$$

where s_{ij} is the component of the compliance tensor, which is the inversion of the stiffness tensor c_{ij}. Components of the stiffness tensor and their temperature (T) coefficients $k_{ij} = \frac{1}{c_{ij}}\frac{\mathrm{d}c_{ij}}{\mathrm{d}T}$ at room temperature are measured;[28] $c_{11} = 167.4$ GPa, $c_{12} = 65.23$ GPa, $c_{44} = 79.57$ GPa, $k_{11} = -75.3$ ppm/°C, $k_{12} = -24.5$ ppm/°C, and $k_{44} = -55.5$ ppm/°C. The temperature coefficients of Young's modulus can be calculated for representative crystal directions

to be −100 ppm/°C in <100>, −70 ppm/°C in <110>, and −55 ppm/°C in <111>. These temperature coefficients become negative in all directions in silicon, which is different from quartz that exhibits a near-zero temperature coefficient in elasticity for some temperature-compensation crystal cuts.[20]

The resonant frequency of the cantilever has, therefore, approximately half the temperature coefficient of Young's modulus according to eq. (1). It is estimated to be between −50 and −27 ppm/°C depending on the crystal orientation, and creates a frequency drift on the order of 10 Hz/°C when the resonant frequency is 1 MHz.

2.2 *p-n junction temperature sensor*

The forward current of the p-n junction diode has been applied to temperature sensors because it exhibits strong temperature dependence. The forward current J against temperature T is expressed as[29]

$$J \propto \exp\left[-\frac{E_g}{k_B T}\right]\exp\left[\frac{qV}{\eta k_B T}\right]. \tag{3}$$

The first exponential term is related to the free carrier density, and E_g and k_B are the band gap energy and Boltzmann constant, respectively. The second exponential term specifies the voltage-current characteristic, where V, q, and η are the forward bias voltage, elementary charge, and ideality factor, respectively. In the case of constant-current operation, the voltage drop of the diode simply becomes a linear function of temperature.

3. Sensor Design and Fabrication

Microcantilevers were fabricated from a 5-μm-thick device layer of a silicon-on-insulator (SOI) wafer. The cantilever had dimensions of 50 μm width and 500 μm length along the <110> direction on the (001) plane. The cantilever structure was formed by deep reactive ion etchings (DRIEs) after photolithographies from both the front and back sides, and followed by sacrificial wet etching of the buried oxide (BOX) layer. The substrate below the cantilever was completely removed to reduce squeezed air damping from the substrate. Top-view and cross-sectional schematics are shown in Fig. 1.

A set of four-bridged piezoresistive gauges (PGs) was fabricated by ion implantation prior to cantilever formation to detect the deflection of the cantilever electrically. The SOI layer was n-type with an impurity concentration of 1×10^{15}/cm^3 . The p-type PG was doped at 5×10^{18}/cm^3 with a thickness of 1 μm, which was electrically isolated by the p-n junction from the SOI layer. Metal wiring of Al-Si-Cu alloy was connected at the contact hole of the passivation layer (500 nm thick), where high-concentration doping (1×10^{19}/cm^3, 0.3 μm thick) was performed to obtain Ohmic contact. Additionally, the contact areas of the n-type SOI layer were also doped (1×10^{19}/cm^3, 0.3 μm thick) to obtain Ohmic contact. The cross section of the device is illustrated in Fig. 1(a).

The top surface of the cantilever was coated with sputtered gold film to enhance adhesion with polymers for molecular detection, as shown in Fig. 1(b). A top-view microscopy image is shown in Fig. 2(a). Of the four PGs, two PGs worked as stress

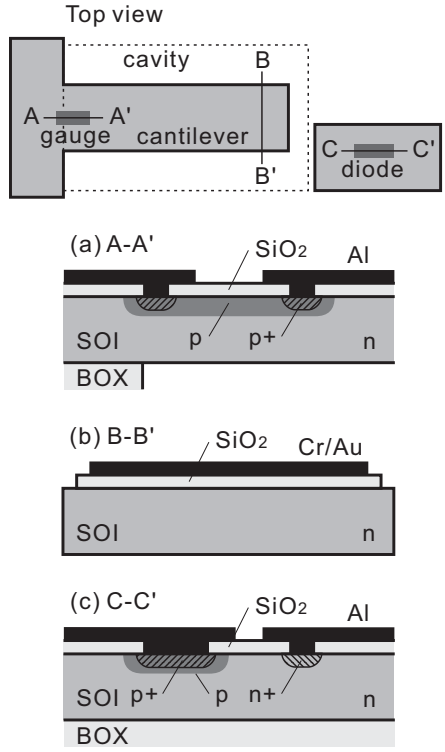

Fig. 1. Schematics of the sensor device. Top figure shows in-plane structure. Figures (a) to (c) show cross-sectional structures of (a) piezoresistive gauge, (b) cantilever, and (c) diode.

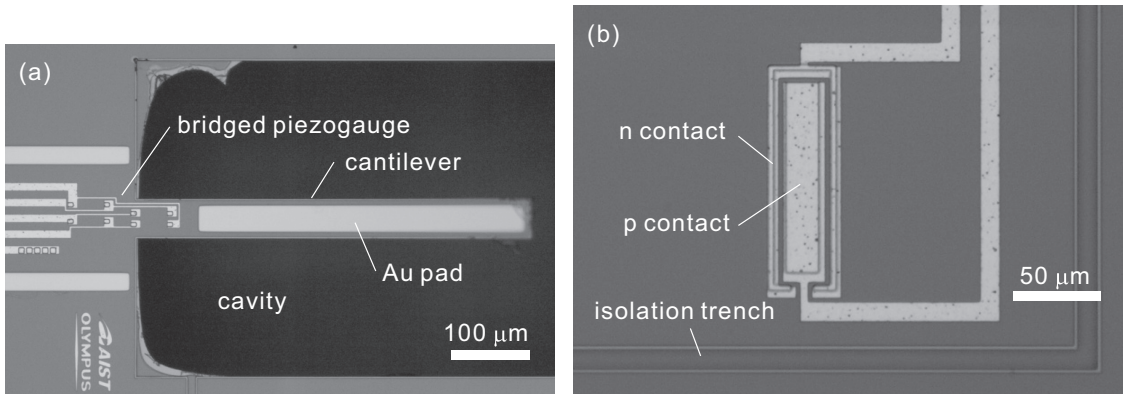

Fig. 2. Microscopy images of (a) cantilever mass sensor and (b) diode temperature sensor.

sensors located at the root of the cantilever and the two other PGs were reference resistors on the substrate. Each PG had a resistance of 6.1 kΩ. Four PGs were used as a Wheatstone bridge in which the output voltage is proportional to the surface stress at the root of the cantilever.

The temperature sensor of the p-n junction diode was also fabricated on the SOI layer by ion implantation, which occupied another area but near to the cantilever in the same chip. The substrate below the diode was not removed. The cross section of the diode is illustrated in Fig. 1(c). The p-type area, the p+ contact, and the n+ contact are formed by the same implantation process for PG. A microscopy image is shown in Fig. 2(b). The n-type device layer was electrically isolated by a trench etched by the same process used to fabricate the cantilever. Therefore, it requires little additional cost to integrate the temperature sensor to the cantilever sensor chip because the fabrication processes were merged to the PG formation processes.

The sensor chip of 5×5 mm^2 area included 8 cantilevers and several diodes, as shown in Fig. 3. The chip was glued on a PZT plate of 0.5 mm thickness using silver paste to provide vibration, and this unit was mounted on a quad flat ceramic package. The PGs, diodes, and PZT plate were electrically connected by gold bonding wires to the package leads. We used two packaged sensor chips for the measurement results in this study. The first sensor chip was used for the basic characterization of the cantilever (CL0) and diode without additional film coating. The second one was assembled in a chemical sensor evaluation system for drift measurement, in which one of the cantilevers (CL1) was used without additional film coating and the other one (CL2) was measured with a polybutadiene (PBD) film coated by microdispensing technique.[30,31] The PBD was chosen as an adsorption material owing to its high sensitivity to VOCs. All the cantilevers CL0, CL1, and CL2 have the same dimensions and film compositions except for the existence of the PBD layer.

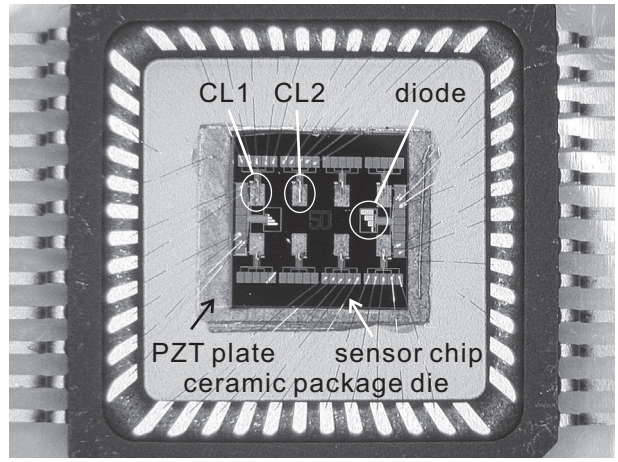

Fig. 3. Microscopy image of packaged sensor chip.

4. Measurement Procedures

4.1 *Basic characteristics*

The basic characteristics of cantilevers and diodes were evaluated using a temperature-controlled chamber, in which the sensor chip was placed. A semiconductor parameter analyzer (Agilent 4155C) was used to examine the voltage-current characteristics of the diode sensor. A network analyzer (Agilent 4395A) was employed to measure the vibration characteristics of the cantilever sensor, where the signal input and output of the analyzer were connected with PZT plate electrodes and the output of the PG, respectively. DC voltage was supplied to the PG bridge from another variable voltage source.

4.2 *Chemical sensing*

A packaged sensor shown in Fig. 3 was used for the experiment of drift compensation during the chemical sensing procedures. The cantilever was driven at around 900 kHz (4th mode) by the use of a feedback oscillation circuit for self-oscillation, which was comprised of a signal amplifier, phase controller, band pass filter, and automatic gain controller.[32] This closed-loop system was developed on the basis of a low-frequency oscillation circuit for a capacitive resonator[33] by improving the frequency bandwidth and selectivity. This circuit allowed us selective oscillation of higher vibration modes of the cantilever up to 1 MHz by adjusting the frequency of the band pass filter. The oscillation frequency was measured using a frequency counter. During the measurement of the frequency shift, the voltage drop in the diode temperature sensor was continuously monitored under constant-current operation.

The packaged sensor was sealed in a closed sensor chamber that was connected to a VOC gas source with a preconcentrator as shown in Fig. 4. The original mixed VOC gas of 0.5 ppm ethanol, 1.8 ppm acetone, and 0.5 ppm toluene diluted in nitrogen carrier gas was led into a preconcentrator at room temperature. Ten liters of the gas was absorbed on carbon fibers in the preconcentrator, and then the gas was desorbed by heating the preconcentrator at 1°C/s with pure nitrogen carrier gas flow. This preconcentrator worked as a kind of thermal chemical separator and generated concentration peaks of ethanol, acetone, and toluene in turn, which is described in detail elsewhere.[30–32]

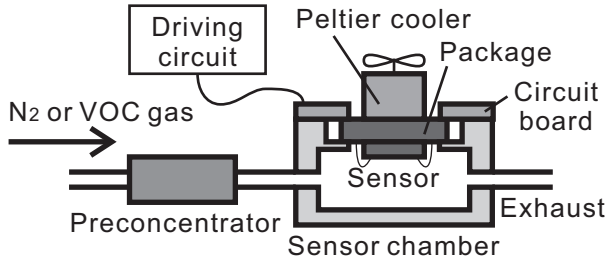

Fig. 4. Experimental setup for VOC detection measurement.

5. Results and Discussion

5.1 *Temperature sensor*

The forward current characteristics of a diode temperature sensor (junction area 6,000 μm^2) at 0, 25, and 50°C are shown in Fig. 5. The measured voltage-current characteristics exhibited approximately straight curves on the semi log plot between 0.4 and 0.7 V, which corresponded to the current between 0.1 μA and 0.1 mA. These curves showed saturation at higher voltages. The current increased markedly depending on the temperature, more than 1 order between 0 and 50°C. As a temperature sensor, constant current operation is useful because the linear response to the temperature is expected. We estimated the sensitivity of the temperature sensor as −2.18 mV/°C at 10 μA operation.

We performed a fitting for the voltage-current curves using eq. (3). The results agreed well with the measurement results below 0.1 mA current as indicated in Fig. 5 by dashed lines, where the parameters were tuned to E_g =1.00 eV and η =1.15. These values imply that our diode can be considered as an ideal diode at the low-current region because the obtained E_g is close to the silicon band gap energy at room temperature (1.12 eV) and η was within normal values (between 1 and 2).

5.2 *Cantilever mass sensor*

The resonance characteristics of the cantilever CL0 were measured around the second resonance mode of flexural vibration at approximately 170 kHz. The reason for the use

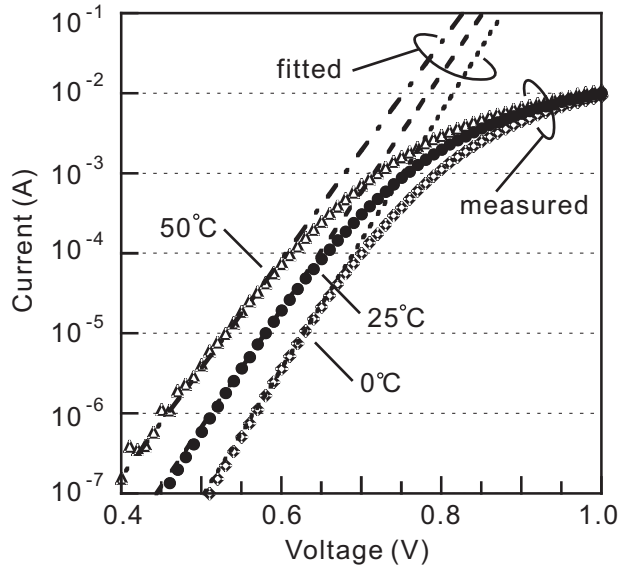

Fig. 5. Voltage-current characteristic of diode temperature sensor at different temperatures.

of the second mode is the lowest frequency limitation of the network analyzer (100 kHz). Firstly, the heating effects of the PG were examined because the DC power consumption might heat the cantilever. We measured resonance curves of the cantilever CL0 placed in a temperature-controlled chamber at 0°C, changing the applied DC voltages V_g to the PG. As shown in Fig. 6, the resonance curves showed a clear resonance curve at 170.2 kHz, and the signal level increased with raised V_g as expected, such that the output voltage is proportional to V_g. When V_g was 7 V, a small peak shift (−10 Hz) from the minimum V_g condition was observed. The higher the increase in V_g, the larger the shift in the frequency peaks. This frequency shift was considered as the result of cantilever heating by PG power, because the shift was roughly proportional to the square of V_g and the power consumption (65 mW) at V_g = 20 V is large enough to heat up floating microscale structures. On the other hand, no heating was observed in the diode temperature sensor because the diode was thermally grounded to the substrate that worked as a heat sink. Therefore, this heating effect was considered to be a local phenomenon limited to a floating cantilever. We chose V_g = 5 V to prevent the heating effect while maintaining sufficient output signals. We expected that the PG heating was not so effective at the design stage because the PGs were located at the cantilever root where the adjacent substrate worked as a heat sink. However, its effect was not actually negligible. In contrast, heating effects due to the temperature sensor could be neglected because the power consumption (70 μW at most in our operation) was much smaller than that of PG.

Figure 7 shows the frequency responses of the cantilever CL0 at three different temperatures, 0, 25, and 50°C. The resonance peak shifted to the lower frequency by

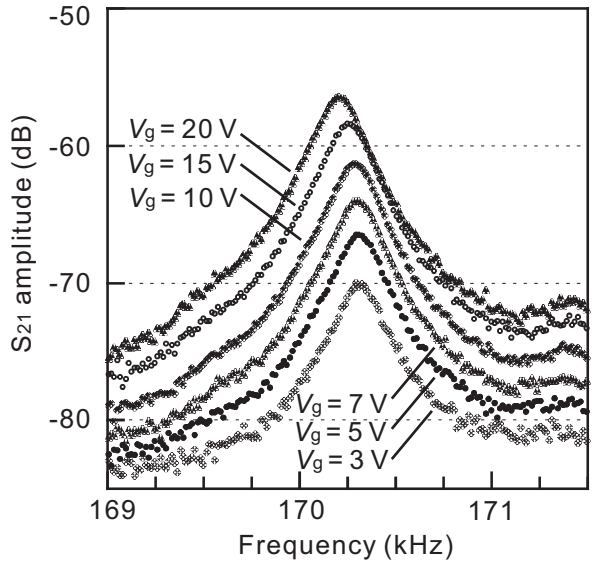

Fig. 6. Frequency response of cantilever mass sensor CL0 at different gauge voltages.

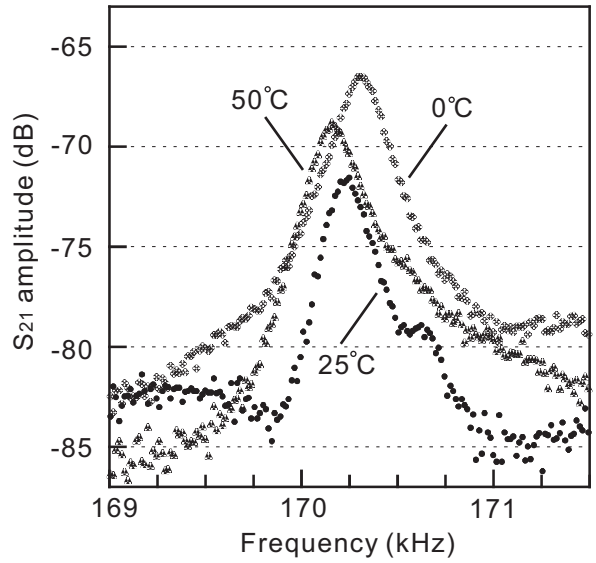

Fig. 7. Frequency response of cantilever mass sensor CL0 at different temperatures.

150 Hz when the temperature was raised from 0 to 50°C, which leads to a frequency coefficient of −18 ppm/°C. The quality factor of the resonance was unchanged. We performed the same procedure on several different resonance modes of different cantilevers and estimated the frequency coefficient to be between −25 and −18 ppm/°C. These values were smaller than the −35 ppm/°C expected from the silicon elasticity. We considered that this difference was mainly the effect of the surface oxide layer because the existence of the oxide film compensated for the temperature effects.[20]

On the other hand, the peak height in Fig. 7 changed irregularly at different temperatures. This phenomenon was considered as the result of temperature effects on the mechanical properties of the PZT plate. The movement of the PZT plate was actually not uniform and provided a complicated vibration shape within the sensor chip in the frequency region that we measured. As a result, the excitation amplitude was not maintained at the same level during the experiment at different temperatures.

5.3 *Drift measurement and compensation*

The long-term drift of the resonance frequency was measured using the self-oscillated cantilever assembled in the sensor evaluation system. Prior to the chemical sensor testing, the frequency drift due to a simple temperature change was examined without gas flow. A Peltier cooler attached to the back side of a sensor package was operated and the changes in cantilever resonance frequency and diode temperature were simultaneously recorded for about 600 s. We used the fourth vibration mode at approximately 900 kHz since our feedback oscillation circuit was optimized around this frequency based on

the result that a higher vibration mode provided higher sensitivity.[30] The temperature effects on the higher vibration modes are basically unchanged from the second mode at 170 kHz because only the coefficient λ becomes larger in eq. (1).

The results of a cantilever CL1 (895 kHz) with a gold surface under a constant gradual cooling condition are shown in Fig. 8(a). The resonant frequency was measured using a frequency counter built in the oscillation circuit. When the temperature of the sensor was slowly lowered at approximately −0.003°C/s, the resonant frequency increased constantly by up to 50 Hz. We evaluated the temperature coefficient of the frequency k_{CL1} as −34 ppm/°C. By using the temperature coefficient k and

$$f_{comp} = (1-k\Delta T) f_{meas}, \tag{4}$$

the compensated frequency f_{comp} is evaluated from the observed frequency f_{meas} and temperature variation ΔT. The frequency shift of as much as 50 Hz could be compensated within ±1 Hz, as shown in Fig. 8(a).

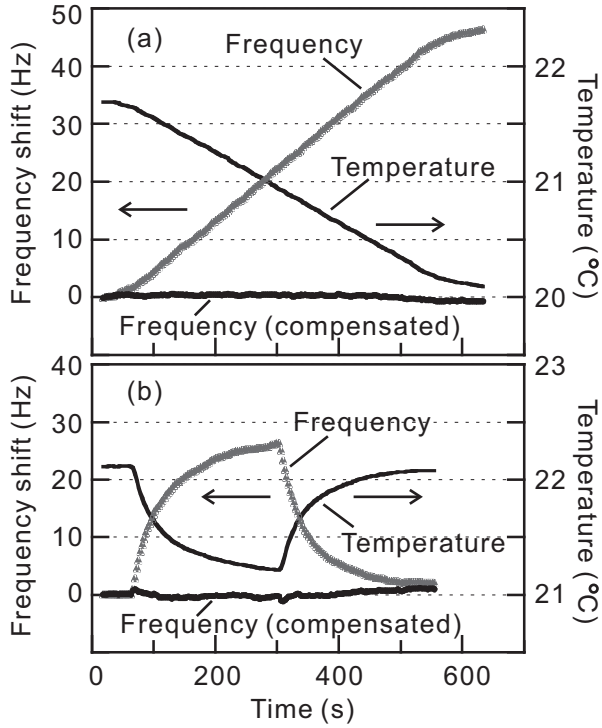

Fig. 8. Long-term frequency drift of cantilever CL1 and its compensation using temperature sensor under (a) gradual cooling and (b) rapid cooling and heating.

The temperature coefficient (−34 ppm/°C) in the oscillation (closed loop) state was slightly larger than that measured by the frequency scan (open loop) method described in the previous section. We considered that this was the effect of the oscillation circuit in which electrical components also had temperature effects. When the phase of the circuit is fluctuated by temperature change, it shifts the oscillation frequency through the movement of the operation point within the resonance band of the resonator.[34] As a result, the temperature coefficients under electrical feedback oscillation are generally different from the original temperature coefficient of the resonator devices. The design of the electric circuit is found to be also important to realize a stable oscillator, although we do not investigate the effects of circuits in this study.

We examined the validity of the compensation under more radical temperature changes up to ±0.02°C/s. Figure 8(b) demonstrates that compensation of around ±1 Hz was also achieved against rapid temperature change even at the abrupt beginning of cooling or heating at ±0.02°C/s. The advantage of an on-chip temperature sensor was proved here because the temperature difference between the cantilever and temperature sensor was minimized in our integrated chip. Only 0.03°C of temperature difference produces a compensation error of 1 Hz when we assumed a cantilever having 895 kHz frequency and −34 ppm/°C coefficient. It is considered very difficult to keep such a small temperature difference between the sensor and a thermometer if an external temperature sensor is used.

A similar procedure was also performed on the PBD-coated cantilever (CL2), and a temperature coefficient $k_{CL2} = -78$ ppm/°C was obtained. The resonant frequency of the cantilever CL2 was lowered to 812 kHz due to the mass effect of the PBD layer. The absolute value of k_{CL2} was twofold larger than k_{CL1} and was considered the effect of the PBD film on the cantilever. As the thickness of the PBD layer (2 μm) was comparable to that of the cantilever, the temperature effects on the elastic properties in the adsorption layer became not negligible. Therefore, the temperature coefficients should be separately measured for different cantilevers with different adsorption layers when we integrate multiple cantilevers in one chip.

5.4 *Resolution of temperature sensor*

From the measured temperature trend in Fig. 8, a part was enlarged in Fig. 9 to observe the measurement resolution. The voltage drop of the diode was measured using a digital multimeter (Yokogawa Electric, 7561) with 500 ms of accumulation time. There was no noiselike signal above 0.01°C and the resolution might be obtained at less than 0.01°C. The standard deviation after filtering the long-term temperature change was roughly estimated to be 0.002°C.

Thermal noise is considered to determine the final resolution of a diode temperature sensor having an equivalent resistance R, and the noise voltage at temperature T is evaluated as

$$V_n = \sqrt{4k_B TRB}\,, \tag{5}$$

where B is the measurement bandwidth. When our diode was operated at 10 μA, its

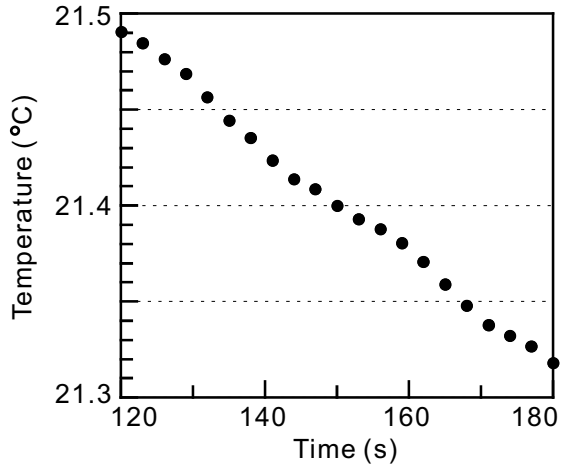

Fig. 9. Enlarged graph of temperature measurement results in Fig. 8(a).

resistance was calculated as 60 kΩ. The noise voltage was evaluated to be 32 nV if we assumed B =1 Hz (corresponding to 1 s sampling) and T = 293 K. This value was equivalent to 1.5×10^{-5} °C for our diode temperature sensor. Therefore, the temperature sensor itself has a capability to measure with a much higher resolution if the voltage measurement apparatus and noise shielding were carefully prepared.

5.5 *Drift under VOC measurement*

This sensor chip integrating two cantilever mass sensors and a temperature sensor was applied to an actual chemical sensing test. We used a preconcentrator as a VOC source from which three types of VOC, ethanol, acetone, and toluene, were desorbed by heating in order of desorption energy.[32] The measured responses are shown in Fig. 10(a). The cantilever CL2 with PBD film responded strongly to acetone and toluene, whereas the CL1 with a gold surface did only weakly to acetone. The frequency shift is considered to be proportional to the adsorbed VOC masses, which are in equilibrium with VOCs in surrounding air.[32] This result demonstrated selective detection using mass sensors of different surfaces. At the same time, these frequency shifts exhibited a large baseline drift comparable to VOC detection signals. We tried the compensation of frequency drift using the temperature coefficients k_{CL1} = −34 ppm/°C and k_{CL2} = −78 ppm/°C obtained by the measurements described above. The temperature sensor exhibited heating during the measurement owing to the gas flow from the hot preconcentrator. The temperature compensation was successfully carried out as shown in Fig. 10(b), where the baseline drift between 15 and 30 Hz was mostly canceled within 2 Hz even after 1,000 s of measurement.

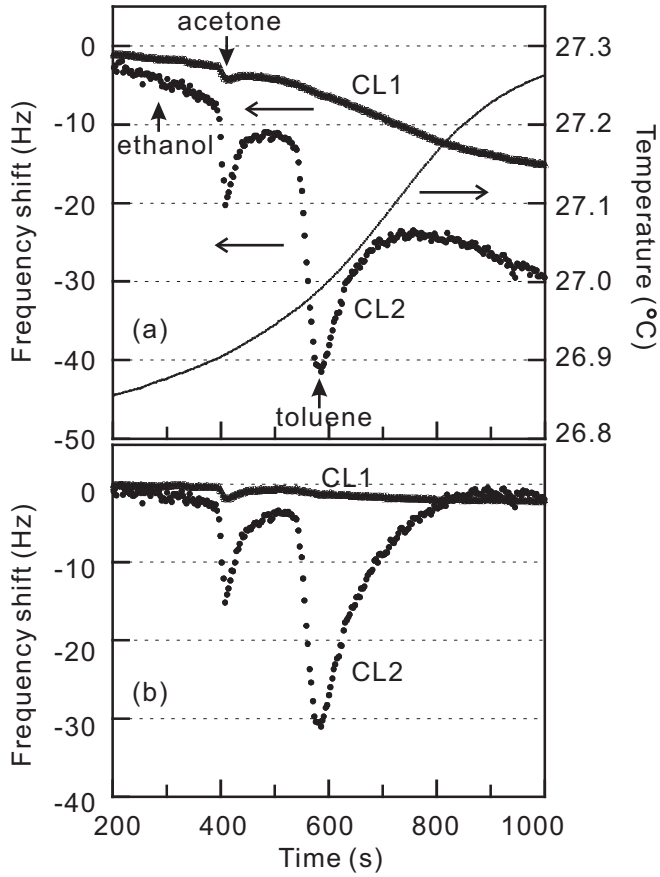

Fig. 10. Frequency shift of two cantilever mass sensors with gold surface (CL1) and polybutadiene-coated surface (CL2) under mixed VOC exposure: (a) raw data and (b) temperature-compensated data.

As we have shown, temperature compensation using an on-chip temperature sensor is expected to reduce the frequency shift and improve the detection limit of the cantilever mass sensor. The flow of carrier gas can easily change the temperature of the sensor; therefore, temperature compensation is inevitably needed for chemical sensing using silicon cantilevers.

6. Conclusions

A p-n junction diode was integrated to a resonant mass sensor using a silicon cantilever in one chip for frequency drift compensation due to temperature fluctuation.

The diode could be fabricated by almost the same fabrication process simultaneously with piezoresistive stress gauges and showed good p-n junction characteristics for a temperature sensor. The sensor chip consisted of multiple cantilevers and the diode was assembled to a sensor package with a PZT vibrator and oscillated using a feedback electric circuit. Frequency drift trends under induced temperature changes could be almost compensated using the temperature read by the on-chip diode and a temperature coefficient. The temperature coefficients were −34 and −78 ppm/°C for gold-coated and polybutadiene-coated cantilevers, respectively, and found to depend strongly on the surface adsorption films on the sensor. Frequency drift compensation under a chemical sensing condition was also demonstrated, which was reduced from the original drift up to 30 Hz to almost 2 Hz. Temperature compensation using an on-chip temperature sensor is considered to be important for chemical sensing using silicon cantilevers where gas flows can easily change the temperature of the sensor.

References

1 G. Sauerbrey: Z. Phys. **155** (1959) 206.
2 M. Kimura, Y. Liu, R. Sakai, S. Sato, T. Hirai, T. Fukawa and T. Mihara: Sens. Mater. **23** (2011) 359.
3 P. Kao, S. Doerner, T. Schneider, D. Allara, P. Hauptmann and S. Tadigadapa : J. Microelectromech. Syst. **18** (2009) 522.
4 F. M. Battiston, J. P. Ramseyer, H. P. Lang, M. K. Baller, Ch. Gerber, J. K. Gimzewski, E. Meyer and H.-J. Güntherodt: Sens. Actuators B **77** (2001) 122.
5 B. H. Kim, F. E. Prins, D. P. Kern, S. Raible and U. Weimar: Sens. Actuators, B **78** (2001) 12.
6 D. Lange, C. Hagleitner, A. Hierlemann, O. Brand and H. Baltes: Anal. Chem. **74** (2002) 3084.
7 J. Jin, X. Li, J. Liu, G. Zuo, Y. Wang, M. Liu and H. Yu: J. Microelectromech. Syst. **16** (2006) 1017.
8 D. Filenko, T. Ivanov, B. E. Volland, K. Ivanova, I. W. Rangelow, N. Nikolov, T. Gotszalk and J. Mielczarski: Rev. Sci. Instrum. **79** (2008) 094101.
9 J. H. Seo and O. Brand: Proceedings of Transducers 2005 (IEEE, Seoul, 2005) p. 593.
10 W. Pang, L. Yan, H. Zhang, H. Yu, E. S. Kim and W. C. Tang: Technical Digest of MEMS 2006 (IEEE, Istanbul, 2006) p. 78.
11 M. Konno, T. Ikehara, J. Lu, R. Maeda and T. Mihara: Technical Digest of 23rd Sensor Symposium (IEEJ, Takamatsu, 2006) p. 249.
12 T. Ikehara, J. Lu, M. Konno, R. Maeda and T. Mihara: J. Microelectromech. Syst. **17** (2007) 2491.
13 R. A. Buser and N. F. de Rooij: Sens. Actuators **17** (1989) 145.
14 H. Muro, H. Kaneko, S. Kiyota and P. J. French: Sens. Actuators, A **34** (1992) 43.
15 Analog Devices: Calibrating iMEMS Gyroscope (Application note AN-1049, available from http://www.analog.com/en/technical-documentation/resources/index.html).
16 K. Harada, K. Ikeda, H. Kuwayama and H. Murayama: Sens. Actuators, A **73** (1999) 261.
17 M. Kimura and K. Toshima: Sens. Actuators, A **108** (2003) 239.
18 S. S. Lee and M. Kimura: Sens. Actuators, A **139** (2007) 104.
19 J. C. Salvia, R. Melamud, S. A. Chandorkar, S. F. Lord and T. W. Kenny: J. Microelectromech. Syst. **19** (2010) 192.
20 R. Melamud, S. A. Chandorkar, B. Kim, H. K. Lee, J. C. Salvia, G. Bahl, M. A. Hopcroft and T. W. Kenny: J. Microelectromech. Syst. **18** (2009) 1409.

21 F. Schoen, M. Nawaz, T. Bever, R. Gruenberger, W. Raberg, W. Weber, B. Winkler and R. Weigel: Technical Digest of MEMS 2009 (IEEE, Sorrento, 2009) p. 884.
22 K. S. Demirci, J. H. Seo, S. Truax, L. A. Beardslee, Y. Luzinova, B. Mizaikoff and O. Brand: Technical Digest of MEMS 2009 (IEEE, Sorrento, 2009) p. 284.
23 R. G. Azevedo, W. Huang, O. M. O'Reilly and A. P. Pisano: Sens. Actuators, A **144** (2008) 374.
24 A. K. Samarao, G. Casinovi and F. Ayazi: Technical Digest of MEMS 2010 (IEEE, Hong Kong, 2010) p. 116.
25 R. D. Blevins: Formulas for Natural Frequency and Mode Shape, Chapter 8 (Krieger Publishing, Malabar, 1979) p. 108.
26 J. J. Wortman and R. A. Evans: J. Appl. Phys. **36** (1965) 153.
27 W. A. Brantley: J. Appl. Phys. **44** (1973) 534.
28 H. J. McSkimin, W. L. Bond, E. Buehler and G. K. Teal: Phys. Rev. **83** (1951) 1080.
29 S. M. Sze: Semiconductor Devices (Wiley, New York, 1987) Chap. 3.
30 T. Mihara, T. Ikehara, J. Lu, R. Maeda, T. Fukawa, M. Kimura, Y. Liu and T. Hirai: AIP Proc. **1137** (2009) 79.
31 T. Mihara, T. Ikehara, M. Konno, R. Maeda, M. Kimura and T. Fukawa: IEEJ Trans. SM **130** (2010) 275.
32 T. Mihara, T. Ikehara, M. Konno, R. Maeda, M. Kimura and T. Fukawa: Sens. Mater. **23** (2011) 397.
33 T. Ikehara and T. Tsuchiya: Sens. Mater. **22** (2010) 39.
34 E. Rubiola: Phase Noise and Frequency Stability in Oscillators (Cambridge University Press, New York, 2009) Chap. 1.